Enhanced active-site electric field accelerates enzyme catalysis

Chu Zheng[†,a], Zhe Ji[†,a], Irimpan I. Mathews[b], and Steven G. Boxer[*,a]

[a]Department of Chemistry, Stanford University, Stanford, CA 94305, USA

[b]Stanford Synchrotron Radiation Lightsource, Menlo Park, CA 94025, USA

†These authors contributed equally to this work.

*Correspondence to: sboxer@stanford.edu

Summary

Enzymes are extraordinarily proficient and selective catalysts arising from billions of years of evolution[1,2]. The rational design of proteins that outperform enzymes especially in their native functions remains a grand challenge. The current *de novo* designed enzymes[3-5] generally exhibit relatively poor activities. This can be improved by directed evolution[4,6-8]; however, this is not grounded in an underlying physical principle. In this work, we exploited the physical principle of electrostatic catalysis[9-11], in which the large electric fields exerted by the charged and polar chemical groups in enzyme active sites preferentially stabilize the more charge-separated transition state over the reactant state and thus accelerate reactions. We report enhancements in electric fields in the active site of horse liver alcohol dehydrogenase (LADH), probed using the vibrational Stark effect, by changing two key features: replacing the serine hydrogen bond donor with threonine (S48T) and replacing the catalytic Zn^{2+} with Co^{2+}. We found that these enhanced electric fields accelerate the rate of hydride transfer, an observation substantially reinforcing the theory of electrostatic catalysis: quantitative predictions can be made beyond the scope of naturally occurring enzymes. The effects of the H-bond and the metal coordination, two distinct chemical forces, can be unified using the same physical quantity — electric field, which is quantitative, and shown here to be additive, and predictive. These results suggest a new design paradigm for both biological and non-biological catalysts.

Main

LADH catalyzes a reversible reaction, either the oxidation of alcohol into aldehydes/ketones by NAD^+ or the reduction of aldehydes/ketones into alcohols by NADH[12]. In the reductive pathway (Fig. 1a), LADH, co-factor NADH, and an aldehyde/ketone substrate form a ternary complex, where the carbonyl (C=O) in the substrate interacts strongly with a catalytic Zn^{2+} and an H-bond donor, S48. The C=O is subject to a nucleophilic attack by the hydride from NADH, proceeding to a transition state with an elongation of the C=O bond and more charge separation along the bond axis. As a result, the C=O in the transition state bears a larger dipole ($\vec{\mu}_{\mathrm{TS}}$) than that in the reactant state ($\vec{\mu}_{\mathrm{RS}}$) (Fig. 1b). An enzyme electric field ($\vec{F}_{\mathrm{enz}}$), created by the elements of the active site, in this case primarily Zn^{2+} and H-bonded S48, interacts with the change in C=O dipole, ($\vec{\mu}_{\mathrm{TS}} - \vec{\mu}_{\mathrm{RS}}$), and could accelerate the hydride transfer reaction by lowering the free energy barrier according to $\Delta\Delta G^{\ddagger} = -\vec{F}_{\mathrm{enz}} \cdot (\vec{\mu}_{\mathrm{TS}} - \vec{\mu}_{\mathrm{RS}})$ (Fig. 1c). The transition state then turns into an oxyanion intermediate before forming the alcohol product (Fig. 1a). In prior experimental studies of other enzymes[10,13], mutations of active-site residues invariably reduce the electric field, slow down the reactions (smaller rate constant k_{cat}), and increase the free energy barrier ($\Delta G^{\ddagger}$). Here we ask whether the field can be made larger and whether $\Delta G^{\ddagger}$ decreases correspondingly (Fig. 1c)? This is an ultimate experimental test of the principle of electrostatic catalysis and its application in designing functional enzymes and catalysts in general.

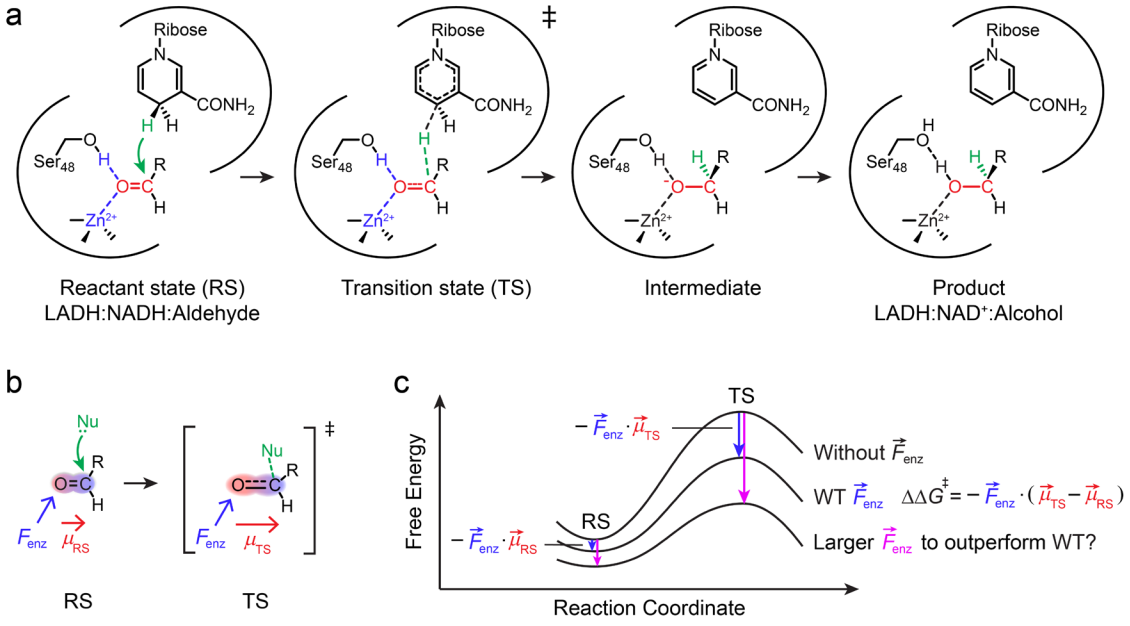

Fig. 1. Electrostatic catalysis of liver alcohol dehydrogenase (LADH). **a**, Mechanism of aldehyde hydrogenation catalyzed by LADH using NADH as the cofactor. **b**, An aldehyde forms the transition state upon a nucleophilic attack. The enzyme active site exerts an electric field ($\vec{F}_{\mathrm{enz}}$) on the carbonyl bond (C=O) dipole, which increases from the reactant state ($\vec{\mu}_{\mathrm{RS}}$) to the more charge-separated transition state ($\vec{\mu}_{\mathrm{TS}}$). **c**, The active site electric field $\vec{F}_{\mathrm{enz}}$ lowers the activation barrier by $\Delta\Delta G^{\ddagger}$ through preferential stabilization of $\vec{\mu}_{\mathrm{TS}}$ over $\vec{\mu}_{\mathrm{RS}}$. Note that the fields are exerted by the charges and dipoles organized by the protein structure itself, not to be confused with an externally applied field[14-17].

As shown in Fig. 2a, the catalytic Zn^{2+} in the LADH active site adopts a tetrahedral coordination geometry comprised of residues of H67, C46, and C174, with the fourth ligand being the C=O of either a substrate or, in the current work, an inhibitor, *N*-cyclohexylformamide (CXF) [18-20]. To modify the electric field exerted by the metal ion, we replaced the active-site Zn^{2+} with other metal ions, including Cd^{2+} and Co^{2+}, by developing a new metal removal-insertion method (Supplementary Methods, Supplementary Fig. 1 and Supplementary Table 1). The metal insertion was optimized by systematically varying the metal ion concentrations and measuring alcohol dehydrogenation activity (Fig. 2b). We obtained the crystal structures of wildtype LADH, $LADH^{Co}$, and $LADH^{Cd}$ (Fig. 2c and Supplementary Table 2). The three structures overlap well, including the coordination geometry of the metal ions, the positioning of NADH, and the length of the H-bond between S48 and the CXF C=O. Zn^{2+} and Co^{2+} are both about 2.2 Å away from the O of the CXF C=O; for Cd^{2+}, this distance is slightly longer at 2.4 Å as expected given the ionic radius. All the metal-O-C angles are ca. 110°.

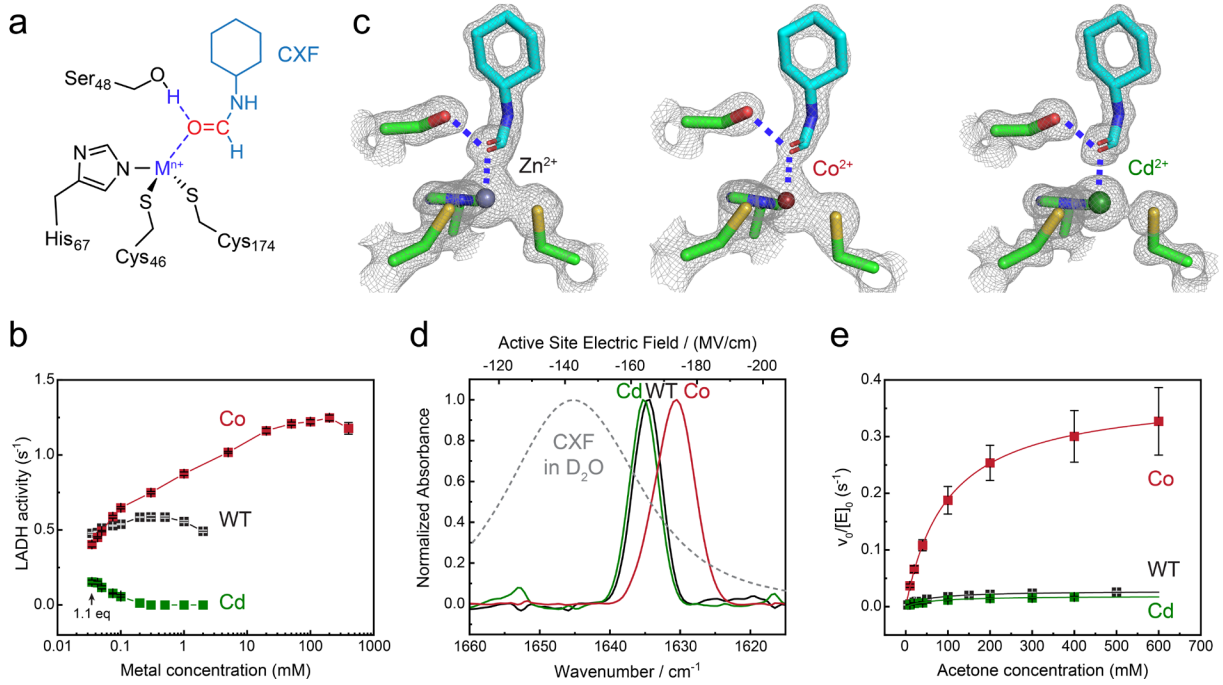

Fig. 2. Metal exchange in the active site of LADH. a, Schematic active site of LADH bound to *N*-cyclohexylformamide (CXF). NADH is omitted for simplicity. **b**, LADH's activity in ethanol dehydrogenation after incubating apo-LADH with the metal ions overnight at 4°C. See Supplementary Methods. The error bars represent one standard deviation of independent triplicates. **c**, Crystal structures of wildtype LADH at 1.43Å resolution (pdb:7RM6), $LADH^{Co}$ at 1.65Å resolution (pdb:8EIW), and $LADH^{Cd}$ at 1.33Å resolution (pdb:7UTW). **d**, Infrared spectra of the C=O in CXF bound to the active site of wildtype LADH, $LADH^{Co}$, and $LADH^{Cd}$. The top electric field axis is mapped from the bottom frequency axis according to: $\bar{\nu} = 0.47F + 1712.2$ (Supplementary Fig. 2), where $\bar{\nu}$ is the wavenumber (cm^{-1}) of the C=O vibrations, and F is the magnitude of electric fields (MV/cm) projected on the C=O. **e**, Michaelis-Menten kinetics of acetone hydrogenation by wildtype LADH, $LADH^{Co}$, and $LADH^{Cd}$. $[E]_0$ was determined by the number of active-site metal ions as quantified by ICP-AES. The error bars represent one standard deviation of independent triplicates. See Supplementary Methods.

To measure electric fields in the active site of LADH, we employed CXF (Fig. 2a), a substrate-analog inhibitor whose C=O stretching vibration can probe the local electrostatic interactions imposed on the aldehyde/ketone substrates by the LADH active site. The calibration of the C=O vibrational probe (Supplementary Methods, Supplementary Fig. 2 and Supplementary Tables 3,4) enables us to utilize the vibrational Stark effect to translate the measured C=O vibrational frequencies into the absolute magnitudes of the electric fields projected onto the C=O bond. Using isotope-edited infrared spectroscopy (Supplementary Methods), we unambiguously identified the C=O vibrational peaks of CXF bound to the wild type and mutants of LADH (Fig. 2d, Supplementary Fig. 3 and Supplementary Table 5). In the wildtype LADH, the C=O frequency of CXF is 1634.6 cm^{-1}, mapping to F_{enz} = -165 MV/cm (the negative sign represents a stabilizing interaction with the C=O dipole), a very large field, considerably larger than the average field for projected on this bond in water (Fig. 2d). For $LADH^{Co}$ and $LADH^{Cd}$, the CXF C=O was redshifted to 1630.6 cm^{-1} and blueshifted to 1635.2 cm^{-1}, respectively, corresponding to a larger field of -174 MV/cm in $LADH^{Co}$ and a slightly smaller field of -163 MV/cm in $LADH^{Cd}$. To elucidate the connection between these electric fields and the hydride transfer in LADH, we measured Michaelis-Menten kinetics of LADH-catalyzed acetone hydrogenation (Supplementary Methods and Supplementary Text 1) which has a rate-limiting hydride transfer reaction[21]. We observed a dramatic 14-fold increase in k_{cat} of acetone hydrogenation by $LADH^{Co}$ compared with $LADH^{Zn}$ (Fig. 2e, Supplementary Fig. 4 and Supplementary Table 6). $LADH^{Cd}$ showed slightly smaller k_{cat} compared to $LADH^{Zn}$.

We next perturbed the H-bond of S48, another key contributor to the active site, by making the S48A and S48T mutants (Fig. 3a). The S48A mutation removed the H-bond interaction and thus significantly blueshifted the C=O band and reduced the active-site electric field projected on the C=O to -139 MV/cm (Fig. 3b, Supplementary Fig. 3 and Supplementary Table 5). By contrast, the S48T mutation redshifted the C=O frequency, leading to a larger field than the wild type of -171 MV/cm. The S48A mutation dramatically decreases the k_{cat} of acetone hydrogenation by 80-fold compared with the wild type, while $LADH^{S48T}$ shows a k_{cat} that is 6.3-fold larger than that of the wild type (Fig. 3c, Supplementary Fig. 4 and Supplementary Table 6). While the S48A mutation directly removes the H-bond, the metal exchange and the S48T mutation did not produce significant structural changes for the bound C=O, as observed from crystallography (Figs. 2c and 3a). Nonetheless, their electrostatic effects can be sensitively reported from direct readouts of vibrational spectroscopy.

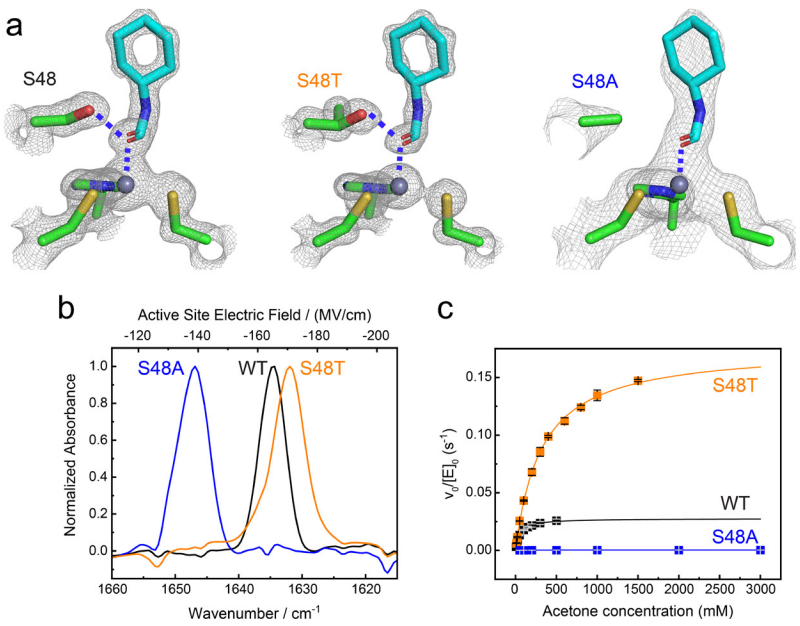

Fig. 3. H-bond perturbation in the active site of LADH. a, Crystal structures of wildtype LADH at 1.43Å resolution (pdb:7RM6), LADH^{S48T} at 1.40 Å resolution (pdb: 7UQ9), and LADH^{S48A} at 2.20 Å resolution (pdb:7U9N), each bound to the inhibitor CXF. See Fig. 2a for the schematic structure. **b**, Infrared spectra of the C=O in CXF bound to the active site of wildtype LADH, LADH^{S48T}, and LADH^{S48A}. See Fig. 2d caption for details. **c**, Michaelis-Menten kinetics of acetone hydrogenation by wildtype LADH, LADH^{S48T}, and LADH^{S48A}. See Fig. 2e caption for details.

As shown in Figs. 4a,b, reaction's free energy barrier ($\Delta G^{\ddagger}$) and the active-site electric field (Supplementary Table 7) show a linear correlation (Supplementary Text 2) over a wide range of both parameters, which indicates that the catalytic effects of the H-bond and the metal ions, despite their different chemical properties, both have a common electrostatic nature and can be quantitatively described using electric fields. In order to test whether the electric field, a physical quantity, is additive, we set out to design double mutants that harness the sum of the effects of single mutants. Specifically, we designed LADH^{Co,S48T} and LADH^{Co,S48A}, and made quantitative predictions for both their fields and activities (Fig. 4c,d). Given that Co^{2+} and S48T mutations enhance the electric fields by -8.5 MV/cm and -5.7 MV/cm, respectively, if the fields are additive, we predicted that LADH^{Co,S48T} would improve the field by -14.2 MV/cm compared to the wild type, reaching -179.4 MV/cm, which would lead to $\Delta G^{\ddagger}$ = 17.5 kcal/mol based on the linear correlation (Fig. 4c). These predictions were found in close agreement with the experimental results (F_{enz} = -180.5 MV/cm; $\Delta G^{\ddagger}$ = 17.1 kcal/mol, Supplementary Fig. 5), resulting in a variant that substantially surpasses the wild type in the rate of hydride transfer: 52-fold for acetone hydrogenation. The other double mutant LADH^{Co,S48A} combines a field-diminishing S48A with a field-enhancing Co^{2+} replacement, which therefore was predicted to rescue the deleterious effect of S48A (Fig. 4d). Indeed, the decrease in electric field (+ 26.2 MV/cm) due to S48A relative to wild type is partially offset by the increase in electric field (-8.5 MV/cm) due to Co^{2+}, resulting in a total field change of +17.7 MV/cm. The predicted F_{enz} = -147.4 MV/cm and $\Delta G^{\ddagger}$ = 21.2 kcal/mol again match well with the experimental results (F_{enz} = -150.2 MV/cm and $\Delta G^{\ddagger}$ = 21.2 kcal/mol, Supplementary Fig. 5). These positive and negative designs clearly demonstrate the additivity of electric fields and a precise electrostatic control of enzyme activities that can both outperform a natural enzyme and fill a continuous activity spectrum (Figs. 4 e,f).

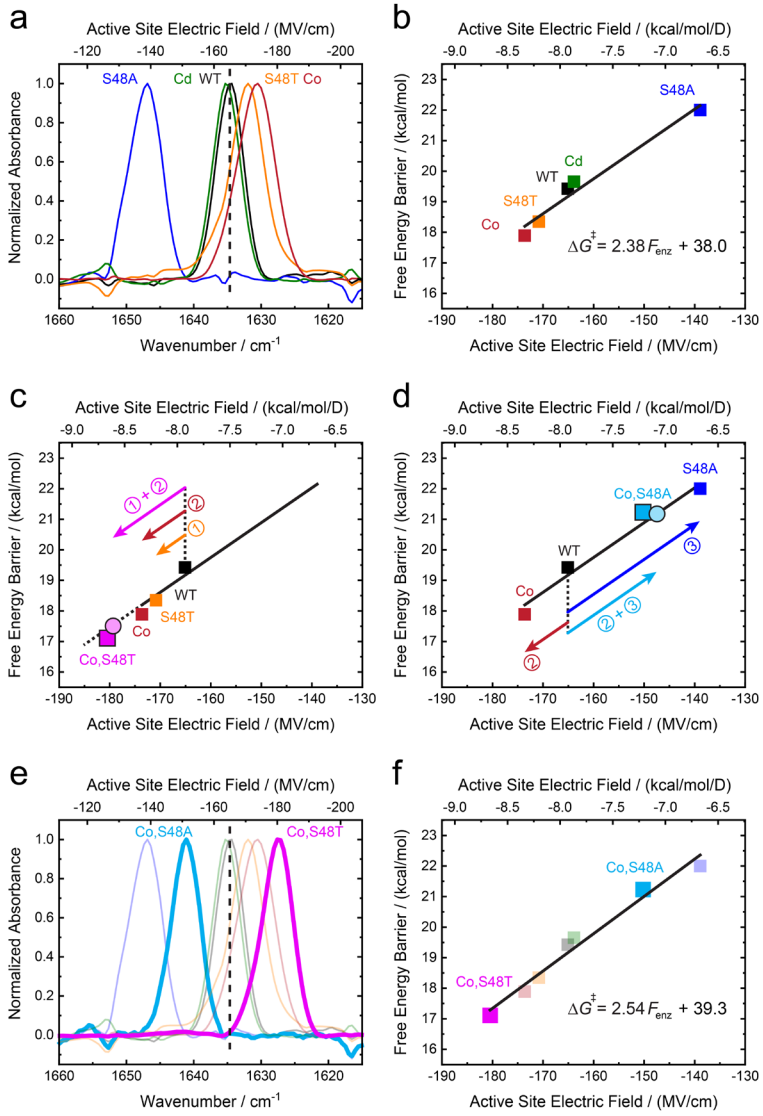

Fig. 4. A unifying electrostatic basis for enzyme catalysis and design. a, Infrared spectra of the C=O in CXF bound to the active site of LADH variants. See Fig. 2d caption for details. **b**, Plot of the free energy barrier ($\Delta G^{\ddagger}$) of acetone hydrogenation against F experienced by the CXF C=O. $\Delta G^{\ddagger}$ was calculated based on transition state theory using k_{cat} determined by kinetic studies (Supplementary Tables 6,7). The linear regression gave $\Delta G^{\ddagger} = 2.38F_{enz} + 38.0$ ($R^2 = 0.97$), with $\Delta G^{\ddagger}$ in kcal/mol and F in kcal/mol/D, a unit manifesting the physical meaning of the slope, which is the reaction difference dipole in Debye (Supplementary Text 2). **c**, Same plot as (b) showing the *prediction* of the double mutant LADH^{Co,S48T} as the sum of the single mutants LADH^{S48T} (①) and LADH^{Co} (②) in terms of F_{enz} and $\Delta G^{\ddagger}$ with respect to the wild type. The prediction (magenta circle) is in close agreement with the experimental data (magenta square). **d**, Same plot as (b) showing the *prediction* of the double mutant LADH^{Co,S48A} as the sum of the single mutants LADH^{Co} (②) and LADH^{S48A} (③) in terms of F_{enz} and $\Delta G^{\ddagger}$ with respect to the wild type. The prediction (blue circle) is in close agreement with the experimental data (blue square). **e**, An extension of (a) including the spectra for the double mutants LADH^{Co,S48T} and LADH^{Co,S48A}. **f**, An extension of (b) by adding the data for the double mutants LADH^{Co,S48T} and LADH^{Co,S48A}. The updated linear regression gave $\Delta G^{\ddagger} = 2.54F_{enz} + 39.3$ ($R^2 = 0.97$).

Discussion

The results summarized in Fig. 4f are striking as they show a linear free energy relationship relating activation free energy to electric field, a physics-based quantity, extending both to slower rates and smaller fields than wild type, but also to larger rates and fields. This suggests a general strategy that has been largely absent[22-25] in the enzyme design community: a focus on the electric field created by the elements of the active site. These same concepts apply to chemical reactivity in general, whether for biological or non-biological reactions in organized environments.

The results show that the hydride transfer reaction of horse LADH can be improved by only a single mutation, changing serine to threonine, or by replacing the catalytic Zn^{2+} with Co^{2+}. Threonine is found at the same site in yeast[26] and human liver[27] alcohol dehydrogenase; however, Co^{2+} unlocks a design space unavailable to nature. Unlike the native incorporation of Zn^{2+} from its micromolar environment *in vivo*, the insertion of Co^{2+} was facilitated by incubating the apo LADH with millimolar Co^{2+} (Fig. 2b), so $LADH^{Co}$ is not expected in nature. The best variant, $LADH^{Co,S48T}$, also outperforms the wild type in carrying out the reverse alcohol dehydrogenation reaction; ethanol, the natural substrate, is transformed 2.4-fold faster (Supplementary Table 8). This reverse reaction has also been studied within the framework of electrostatic catalysis, though its mechanism is more complicated than the hydride transfer step (Supplementary Text 3 and Supplementary Figs. 6,7), and our carbonyl probe relates most directly to the hydride transfer step.

The language of electric fields has been used to describe H-bonds, halogen-bonds, dipole-dipole interactions, and induced dipole interactions,[28] but to date not coordinate bonds. Our results show that the metal–carbonyl coordination in the active site of LADH, where the metal is Zn^{2+}, Cd^{2+}, or Co^{2+} and the carbonyl is a part of an aldehyde or ketone (Fig. 1a), can also be treated within this framework. This simple, classical picture allows us to analyze *local* interactions that are less accessible from theories like ligand field theory[29], which addresses the *global* symmetry and properties of coordination complexes. The electric field is also a different language from Lewis acidity as the strength of Lewis acidity is a *relative* quantity[30], often entangled with that of Lewis basicity of the Lewis adduct partner[31]. In contrast, electric field explicitly describes the energetic effect of a metal ion on a ligand bond dipole on an *absolute* scale and with physics-based units. Most importantly, while concepts like Lewis acidity are validated by thermodynamics (free energy changes and equilibrium constants), the active-site electric field can address functionally relevant kinetics because it directly affects both the bond dipoles of the reactant and transition states (Fig. 1b & c).

The ability of our electrostatic model to capture the faster-than-wildtype reactions in $LADH^{Co}$, $LADH^{S48T}$, and $LADH^{Co,S48T}$ reinforces the importance and universality of electrostatic catalysis as a basic physical principle applicable beyond the scope of naturally occurring enzymes and as a useful design principle for directed evolution and protein engineering. Given the power of electric fields for describing molecular interactions in a local and absolute manner, and the additive[32] and quantitative nature of these fields, together with the rapid developments of *de novo* protein design programs[3-5,33,34] and computational tools[22-25], we envision a promising future within reach to fully

harness the power of electrostatic catalysis to design faster enzymes beyond the natural ones, as well as chemical catalysts that are widely used.

Data availability

The x-ray coordinates and structural factors of LADH variants complexed with NADH and CXF have been deposited in the Protein Data Bank as entries 7UQ9 ($LADH^{S48T}$), 8EIW ($LADH^{Co}$), 7UTW ($LADH^{Cd}$), 7U9N ($LADH^{S48A}$), 8EIY ($LADH^{Co,S48T}$), and 8EIX ($LADH^{Co,S48A}$). All the data that support the finding of this study are available within this article and its Supplementary Information.

Acknowledgements

We thank B.V. Plapp at the University of Iowa for providing detailed guidance on the expression and purification of LADH and much other valuable advice. We thank I. Andersson at Uppsala University and W. Maret at King's College London for their advice on the metal substitution of LADH. We thank A. Braun, A. Heyer, and M. Brueggemeyer for the data analysis and discussion of $LADH^{Co}$; G. Li at the Stanford Environmental Measurements Facility (EMF) for the data collection of ICP-AES; T. McLaughlin from Stanford University Mass Spectrometry (SUMS) for the measurements of native mass spectrometry; T. Carver at the Stanford Nano Shared Facilities (SNSF) for nickel coating Stark windows. C.Z. is grateful for a Stanford Center for Molecular Analysis and Design (CMAD) Fellowship. This work was supported by NIH Grant GM118044 (to S.G.B.). Use of the Stanford Synchrotron Radiation Lightsource, SLAC National Accelerator Laboratory, is supported by the U.S. Department of Energy, Office of Science, Office of Basic Energy Sciences under Contract No. DE-AC02-76SF00515. The SSRL Structural Molecular Biology Program is supported by the DOE Office of Biological and Environmental Research, and by the National Institutes of Health, National Institute of General Medical Sciences (P30GM133894). The contents of this publication are solely the responsibility of the authors and do not necessarily represent the official views of NIGMS or NIH.

Author contributions

C.Z. and S.G.B. designed the research. C.Z. and Z.J. performed most of the experiments and data analysis, including expression and purification of LADH variants, metal substitution of LADH, infrared spectroscopy, and enzyme kinetic studies. C.Z. and I.I.M. performed x-ray crystallography and solved the crystal structures of LADH variants. C.Z., Z.J., and S.G.B discussed the results and wrote the manuscript.

Corresponding authors

Correspondence to Steven G. Boxer (sboxer@stanford.edu).

Competing interests

The authors declare no competing interests.

References

1 Radzicka, A. & Wolfenden, R. A proficient enzyme. *Science* **267**, 90-93 (1995).

2 Risso, V. A., Gavira, J. A., Mejia-Carmona, D. F., Gaucher, E. A. & Sanchez-Ruiz, J. M. Hyperstability and substrate promiscuity in laboratory resurrections of precambrian β-lactamases. *J. Am. Chem. Soc.* **135**, 10580-10580 (2013).

3 Huang, P. S., Boyken, S. E. & Baker, D. The coming of age of de novo protein design. *Nature* **537**, 320-327 (2016).

4 Kries, H., Blomberg, R. & Hilvert, D. De novo enzymes by computational design. *Curr. Opin. Chem. Biol.* **17**, 221-228 (2013).

5 Lovelock, S. L. *et al.* The road to fully programmable protein catalysis. *Nature* **606**, 49-58 (2022).

6 Arnold, F. H. & Volkov, A. A. Directed evolution of biocatalysts. *Curr. Opin. Chem. Biol.* **3**, 54-59 (1999).

7 Bunzel, H. A. *et al.* Evolution of dynamical networks enhances catalysis in a designer enzyme. *Nat. Chem.* **13**, 1017-1022 (2021).

8 Otten, R. *et al.* How directed evolution reshapes the energy landscape in an enzyme to boost catalysis. *Science* **370**, 1442-1446 (2020).

9 Warshel, A. *et al.* Electrostatic basis for enzyme catalysis. *Chem. Rev.* **106**, 3210-3235 (2006).

10 Fried, S. D., Bagchi, S. & Boxer, S. G. Extreme electric fields power catalysis in the active site of ketosteroid isomerase. *Science* **346**, 1510-1514 (2014).

11 Fried, S. D. & Boxer, S. G. Electric fields and enzyme catalysis. *Annu. Rev. Biochem.* **86**, 387-415 (2017).

12 Plapp, B. V. *et al.* Horse liver alcohol dehydrogenase: Zinc coordination and catalysis. *Biochemistry* **56**, 3632-3646 (2017).

13 Schneider, S. H. & Boxer, S. G. Vibrational Stark effects of carbonyl probes applied to reinterpret IR and Raman data for enzyme inhibitors in terms of electric fields at the active site. *J. Phys. Chem. B* **120**, 9672-9684 (2016).

14 Shaik, S., Danovich, D., Joy, J., Wang, Z. & Stuyver, T. Electric-field mediated chemistry: Uncovering and exploiting the potential of (oriented) electric fields to exert chemical catalysis and reaction control. *J. Am. Chem. Soc.* **142**, 12551-12562 (2020).

15 Shaik, S., Mandal, D. & Ramanan, R. Oriented electric fields as future smart reagents in chemistry. *Nat. Chem.* **8**, 1091-1098 (2016).

16 Aragones, A. C. *et al.* Electrostatic catalysis of a diels-alder reaction. *Nature* **531**, 88-91 (2016).

17 Zang, Y. P. *et al.* Directing isomerization reactions of cumulenes with electric fields. *Nat. Commun.* **10** (2019).

18 Deng, H., Schindler, J. F., Berst, K. B., Plapp, B. V. & Callender, R. A Raman spectroscopic characterization of bonding in the complex of horse liver alcohol dehydrogenase with NADH and N-cyclohexylformamide. *Biochemistry* **37**, 14267-14278 (1998).
19 Ramaswamy, S., Scholze, M. & Plapp, B. V. Binding of formamides to liver alcohol dehydrogenase. *Biochemistry* **36**, 3522-3527 (1997).
20 Zheng, C. *et al.* A two-directional vibrational probe reveals different electric field orientations in solution and an enzyme active site. *Nat. Chem.* **14**, 891-897 (2022).
21 Adolph, H. W., Kiefer, M. & Zeppezauer, M. in *Enzymology and molecular biology of carbonyl metabolism 4* (eds Henry Weiner, David W. Crabb, & T. Geoffrey Flynn) 401-410 (Springer US, 1993).
22 Vaissier, V., Sharma, S. C., Schaettle, K., Zhang, T. R. & Head-Gordon, T. Computational optimization of electric fields for improving catalysis of a designed kemp eliminase. *ACS Catal.* **8**, 219-227 (2018).
23 Vaissier Welborn, V. & Head-Gordon, T. Computational design of synthetic enzymes. *Chem. Rev.* **119**, 6613-6630 (2019).
24 Welborn, V. V., Ruiz Pestana, L. & Head-Gordon, T. Computational optimization of electric fields for better catalysis design. *Nat. Catal.* **1**, 649-655 (2018).
25 Hennefarth, M. R. & Alexandrova, A. N. Direct look at the electric field in ketosteroid isomerase and its variants. *ACS Catal.* **10**, 9915-9924 (2020).
26 Raj, S. B., Ramaswamy, S. & Plapp, B. V. Yeast alcohol dehydrogenase structure and catalysis. *Biochemistry* **53**, 5791-5803 (2014).
27 Niederhut, M. S., Gibbons, B. J., Perez-Miller, S. & Hurley, T. D. Three-dimensional structures of the three human class i alcohol dehydrogenases. *Protein Sci.* **10**, 697-706 (2001).
28 Fried, S. D. & Boxer, S. G. Measuring electric fields and noncovalent interactions using the vibrational Stark effect. *Acc. Chem. Res.* **48**, 998-1006 (2015).
29 Griffith, J. S. & Orgel, L. E. Ligand-field theory. *Quarterly Reviews* **11**, 381-393 (1957).
30 Anslyn, E. V. & Dougherty, D. A. *Modern physical organic chemistry*. (University Science, 2006).
31 Drago, R. S., Vogel, G. C. & Needham, T. E. 4-parameter equation for predicting enthalpies of adduct formation. *J. Am. Chem. Soc.* **93**, 6014-& (1971).
32 Lin, C. Y., Romei, M. G., Mathews, I. I. & Boxer, S. G. Energetic basis and design of enzyme function demonstrated using GFP, an excited-state enzyme. *J. Am. Chem. Soc.* **144**, 3968-3978 (2022).
33 Anishchenko, I. *et al.* De novo protein design by deep network hallucination. *Nature* **600**, 547-552 (2021).
34 Wang, J. *et al.* Scaffolding protein functional sites using deep learning. *Science* **377**, 387-394 (2022).